ACS APPLIED ENGINEERING MATERIALS

pubs.acs.org/acsaenm

Article

Microcrystalline Cellulose-Infused Additive Manufactured Filaments: A Sustainable Path to Enhancing Electrochemical Sensors

Published as part of ACS Applied Engineering Materials special issue "Additive Manufacturing for Energy and Environment".

Bruno Ferreira, Elena Bernalte, Robert D. Crapnell, Karen K. L. Augusto, Uday Lomesh, Muhzamil A. Khan, Orlando Fatibello-Filho, Thiago R.L.C. Paixão, and Craig E. Banks*

Cite This: ACS Appl. Eng. Mater. 2025, 3, 1759–1769

Read Online

ACCESS | Metrics & More | Article Recommendations | Supporting Information

ABSTRACT: Additive manufacturing is an inherently low-waste manufacturing technology and the development of printable materials in a sustainable way is vital for the method to thrive and align with the United Nations Sustainable Development Goals. This study advances the field of additive manufacturing electrochemistry by uniquely producing an electrically conductive printable material, improving both sustainability and electrochemical performance. Through the innovative combination of microcrystalline cellulose, carbon black, biobased castor oil and recycled poly(lactic acid), a highly conductive, printable filament was produced. The incorporation of microcrystalline cellulose reduces the plastic content of the filament by 10 wt % while demonstrating a reduced resistance, making this filament a promising candidate for various applications that require conductivity. The additively manufactured electrodes with microcrystalline cellulose were electrochemically benchmarked against other additively manufactured electrodes without microcrystalline cellulose. The microcrystalline cellulose filament (20 wt % carbon black/10 wt % microcrystalline cellulose/10 wt % castor oil/60 wt % recycled poly(lactic acid)) produced a heterogeneous rate constant (k^0_{obs}) of 0.35 (±0.03) × 10^{-3} cm s^{-1} and a charge transfer resistance (R_{ct}) of 207 ± 32 Ω, compared to k^0_{obs} of 0.27 (±0.03) × 10^{-3} cm s^{-1} and R_{ct} = 579 ± 32 Ω for the filament with no microcrystalline cellulose added. The microcrystalline cellulose filament was successfully used to create an eco-friendly electroanalytical sensing platform to detect dopamine, obtaining good values of linearity, ranging from 0.01 to 1 μM, a sensitivity of 7.943 μA $μM^{-1}$, and a limit of detection (LOD) and quantification (LOQ) of 3 and 10 nM, respectively, before successfully being applied within a spiked human serum sample, obtaining recoveries of 102.4%. Overall, this work marks a significant advancement in the development of eco-friendly materials for additive manufacturing, contributing both to improved technological performance and the sustainability of the additive manufacturing industry.

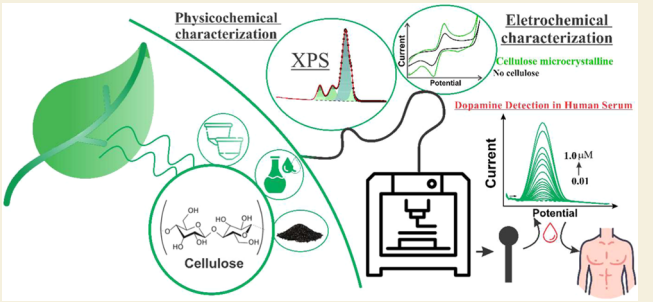

KEYWORDS: *additive manufacturing, microcrystalline cellulose, low-cost, electroanalysis, eco-friendly, dopamine*

1. INTRODUCTION

Additive manufacturing electrochemistry has gained popularity as an emerging field due to its low entry costs, minimal waste production, high level of customization, and global connectivity. Fused Filament Fabrication (FFF), also known as Fused Deposition Modeling (FDM), is the most widely used technique in this field, mainly because of its cost-effectiveness and the widespread availability of conductive filament. FFF deposits thermoplastic material in thin, successive layers to create a fully formed three-dimensional (3D) object. This technique has already been utilized in various areas, such as sensors, energy storage, environmental analyses, and forensic analyses.[1−5]

Poly(lactic acid) (PLA), a biodegradable polymer under industrial conditions, is widely used for FFF due to its excellent printability and simple processing. When combined with conductive materials and suitable plasticizers, highly conductive printable filaments can be produced. Although inherently low-waste, FFF still utilizes mainly plastic sources. Therefore, efforts to improve its environmental sustainability are vital to ensure it remains aligned with the United Nations Sustainable Development Goals, in particular Goal 12, "Responsible Consumption and Production".[6]

Received: March 27, 2025
Revised: May 22, 2025
Accepted: May 23, 2025
Published: June 4, 2025

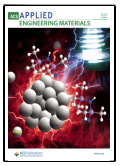

Researchers have recently shown that PLA can be substituted for recycled PLA (rPLA), creating a unique circular economy electrochemistry, whereby waste plastic from coffee pods was recycled into sensors for the detection of caffeine within coffee and tea samples.[7] Plasticizers are another crucial component of producing conductive filaments with PLA. They help to maintain the high mass of conductive material while maintaining the flexibility of these filaments at low temperatures. In the literature, poly(ethylene glycol) (PEG) is one of the most commonly used plasticizers for PLA. This compound is utilized in battery and capacitor research primarily due to its low melting and glass transition temperature.[8−10] The search for biobased plasticizers is important to improve sustainability, decrease toxicity, and decrease the cost of the filament. Castor oil (CO) is a nonedible oil obtained from the seeds of the *Ricinus communis* (*Euphorbiaceae* family) plant.[11] The oil extraction process can be done through mechanical pressing or solvent extraction. Conductive filaments with CO have already been employed in various research for the quantification of bisphenol A (BPA) in bottled and tap water, trinitrotoluene (TNT) in explosives, and the determination of β-estradiol within environmental waters.[8,10,12]

Cellulose is a significant macromolecule that plays an essential role in the structural integrity of plants. It is the most abundant natural polymer on Earth and is a linear polysaccharide. It exists in two forms: crystalline, characterized by a highly organized arrangement of molecules, and amorphous, more irregular, and disordered. Predominantly found in plant tissues, cellulose provides strength and support, serving as the primary structural component of plant cell walls.[13] Moreover, cellulose is a versatile and renewable biopolymer composed of β-1,4-linked anhydro-D-glucose units. This natural compound is abundant in various plants, including cotton, bamboo, and wood, as a fundamental structural component. Due to the unique structure of cellulose, which is characterized by its extensive hydrogen bonding, it can impart excellent mechanical strength and thermal stability. In addition to this, its renewable nature, versatility and functional properties have seen it gain significant interest within additive manufacturing and sensor development. For example, cellulose based hydrogels have been extensively explored for the development of flexible and wearable sensors for temperature, pressure and humidity.[14] The use of cellulose within electrochemical sensors for medical diagnostics, environmental monitoring and wearable technology has also been reported.[15]

Each year, approximately 1.5 trillion tons of biomass are produced globally, with cellulose constituting a significant portion of this total. This vast availability highlights cellulose's potential as an underutilized resource, positioning it as a key player in sustainable practices and ecological applications.[16] Moon and colleagues classified cellulose into six distinct groups based on their structure and morphology: cellulose microfibre (MF), microcrystalline cellulose (MCC), cellulose nanocrystalline (CNC), nanofibrillated cellulose (NFC), bacterial cellulose particles (BC), and regenerated cellulose (RC).[13,17] MCC is composed of porous particles that vary in size from 10 to 50 μm. This material exhibits remarkable crystallinity, achieved by eliminating the amorphous regions through acid hydrolysis. The crystalline structure of MCC emerges from the intricate interplay of van der Waals forces and hydrogen bonds that connect adjacent cellulose chains. This unique arrangement contributes to the stability and integrity of the material.

Furthermore, MCC boasts a significantly higher surface area than other cellulose types, enhancing its reactivity and versatility in various applications.[18] Due to its unique properties, MCC has become an important commercial product, widely utilized across multiple industries, including pharmaceuticals, cosmetics, and food production.[19] Combining PLA with a biopolymer such as cellulose is a practical approach for enhancing the key properties of filament material. This can lead to modifications in the thermal, mechanical, degradability, and cost-related aspects of PLA filament.[19] However, the challenge lies in achieving homogeneity in the manufactured filaments when blending PLA with cellulose, primarily due to the contrasting characteristics of the molecules involved. While PLA is inherently hydrophobic, cellulose has abundant hydrophilic functional groups (−OH) on its surface.[16]

PLA and MCC have been utilized to develop nonconductive filaments for additive manufacturing, enhancing its final characteristics. Including MCC in the PLA filament has shown improvements in various physical properties. Specifically, when MCC is well-dispersed throughout the formulation, it contributes to enhanced tensile modulus, thermal stability, and crystallinity.[16,19] It has been shown that the addition of as low as 1 wt % MCC can improve the mobility of PLA chains, while enhancing the elasticity and tensile strength of wood-PLA composite filaments.[20] Similarly, the addition of 12 wt % MCC to PLA has been shown to increase the storage modulus of the material at 35 °C by over 45%.[21]

As such, in this study, we look to apply this concept t the development of a novel conductive filament for the first time. We uniquely combine microcrystalline cellulose and recycled PLA, using carbon black as conductive filler, castor oil as biobased plasticizer and without using organic solvents. This work highlights how processes and materials can be made more sustainable, while improving the final product's performance.

2. EXPERIMENTAL SECTION

2.1. Chemicals

All chemicals used throughout this work were used as received without any further purification. All aqueous solutions were prepared with deionized water of a measured resistivity of 18.2 MΩ·cm, sourced from a Milli-Q Integral 3 system from Millipore U.K. (Watford, U.K.). Hexaammineruthenium(III) chloride ($[Ru(NH_3)_6]^{3+}$, 98%), potassium ferricyanide ($[Fe(CN)_6]^{3-}$, 99%), potassium ferrocyanide ($[Fe(CN)_6]^{4-}$, 98.5−102%), sodium hydroxide (>98%), potassium chloride (99.0−100.5%), poly(ethylene glycol) (PEG3000), castor oil (CO), microcrystalline cellulose (MCC-99%), acetaminophen (≥99%), phenylephrine hydrochloride (≥99%), β-nicotinamide adenine dinucleotide (NADH, ≥97%), sodium nitrite (≥97%), dopamine hydrochloride (DPA, ≥99%), Human Serum (Male AB, sterile-filtered) and phosphate-buffered saline (PBS) tablets were purchased from Merck (Gillingham, U.K.). Carbon black (CB) was purchased from Pi-kem (Tamworth, U.K.). Recycled poly(lactic acid) (rPLA) was purchased from Gianeco (Italy). Commercial conductive PLA/carbon black filament (1.75 mm, ProtoPasta, Vancouver, Canada).

2.2. Filament Production

All rPLA was dried in an oven at 60 °C for 2.5 h to remove residual moisture from the polymer. The polymer compositions were prepared by combining appropriate amounts of rPLA, CB, CO/PEG3000, and MCC in a 63 cm^3 mixing chamber. The materials were blended using a Thermo Haake Polydrive dynameter equipped with a Thermo

https://doi.org/10.1021/acsaenm.5c00233
ACS Appl. Eng. Mater. 2025, 3, 1759−1769

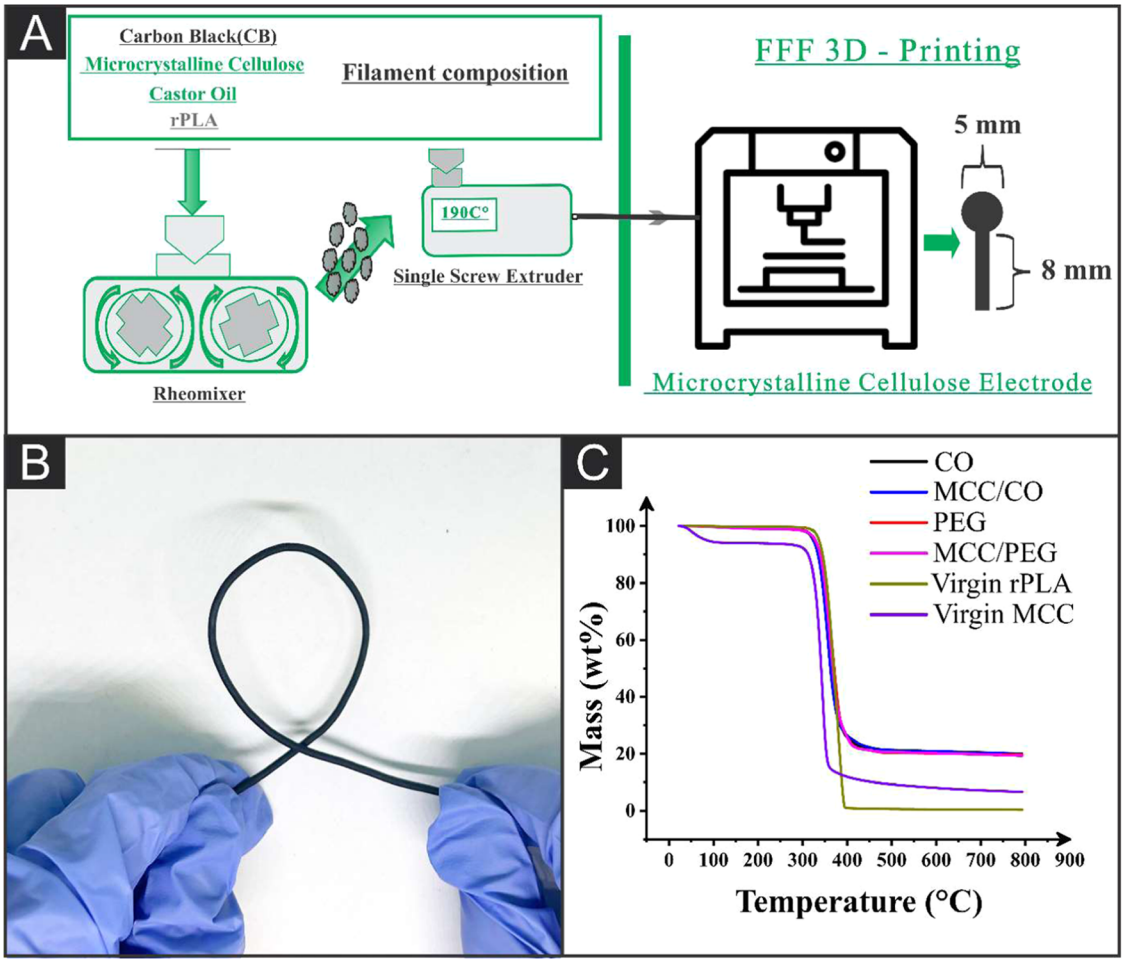

Figure 1. (A) Schematic of filament production. (B) Photograph of the MCC/CO filament highlighting the excellent low-temperature flexibility. (C) TGA analysis of the different filaments compared to the virgin rPLA and virgin MCC.

Haake Rheomix 600 (Thermo-Haake, Germany) at 190 °C with Banbury rotors set to 70 rpm for 5 min. Once mixed, the polymer composites were allowed to cool to room temperature before being granulated to achieve a finer particle size using a Rapid Granulator 1528 (Rapid, Sweden). The resulting composites were then processed through the hopper of an EX2 extrusion line (Filabot, VA). The EX2 was configured with a single screw and a set heat zone of 190 °C. The molten polymer was extruded through a 1.75 mm die head, pulled along an Airpath cooling line (Filabot, VA), and collected onto a spool. The filament was then ready for use in additive manufacturing.

2.3. Additive Manufacturing of the Electrodes

All computer designs and 3MF files in this manuscript were produced using Fusion 360 (Autodesk, CA). These files were sliced and converted to GCODE files in PrusaSlicer (Prusa Research, Prague, Czech Republic). The additive-manufactured electrodes were produced using fused filament fabrication (FFF) technology on a Prusa i3MK3S+ (Prusa Research, Prague, Czech Republic). All additive-manufactured electrodes were printed using identical printing parameters: a 0.6 mm nozzle with a nozzle and bed temperature of 215 and 60 °C, respectively. The rectilinear infill was 100%, 0.15 mm layer height, and print speed of 35 mm s^{-1}.

2.4. Physicochemical Characterization

Thermogravimetric analysis (TGA) was performed using a Discovery Series SDT 650 controlled by Trios Software (TA Instruments, DA). Samples were mounted in alumina pans (90 μL) and tested using a ramp profile (10 °C min^{-1}) from 0−800 °C under N_2 (100 mL min^{-1}).

X-ray Photoelectron Spectroscopy (XPS) data were acquired using an AXIS Supra (Kratos, U.K.) equipped with a monochromatic Al X-ray source (1486.6 eV) operating at 225 W and a hemispherical sector analyzer. It was operated in fixed transmission mode with a pass energy of 160 eV for survey scans and 20 eV for region scans with the collimator operating in slot mode for an analysis area of approximately 700 × 300 μm^2, the fwhm of the Ag 3d5/2 peak using a pass energy of 20 eV was 0.613 eV. The binding energy scale was calibrated by setting the graphitic sp^2 C 1s peak to 284.5 eV; this calibration is considered flawed but was nonetheless used without reasonable alternatives and because only limited information was inferred from absolute peak positions.

Scanning Electron Microscopy (SEM) micrographs were obtained using a Crossbeam 350 Focused Ion Beam − Scanning Electron Microscope (FIB-SEM) (Carl Zeiss Ltd., Cambridge, U.K.) fitted with a field emission electron gun. Secondary electron imaging was completed using a Secondary Electron Secondary Ion (SESI) detector. Samples were mounted on the aluminum SEM pin stubs (12 mm diameter, Agar Scientific, Essex, U.K.) using adhesive carbon tabs (12 mm diameter, Agar Scientific, Essex, U.K.) and coated with a 5 nm layer of Au/Pd metal using a Leica EM ACE200 coating system before imaging.

2.5. Electrochemical Experiments

All electrochemical experiments were conducted using an Autolab PGSTAT 204 potentiostat controlled by NOVA 2.1.7 software (Utrecht, The Netherlands). Identical additive-manufactured electrodes, shaped like lollipops (Ø 5 mm disc with an 8 mm connection length, 2 mm width, and 1 mm thickness[24]), were employed consistently for all filaments, alongside an external commercial Ag|

https://doi.org/10.1021/acsaenm.5c00233
ACS Appl. Eng. Mater. 2025, 3, 1759−1769

AgCl|KCl (3M) reference electrode and a nichrome wire counter electrode. Before each electrochemical experiment, all solutions of $[Ru(NH_3)_6]^{3+}$ were thoroughly purged of O_2 using nitrogen. Solutions of $[Fe(CN)_6]^{4-/3-}$ were prepared similarly without requiring additional degassing.

Electrochemical impedance spectroscopy (EIS) was performed in the frequency range of 0.1 Hz to 100 kHz, applying a signal amplitude of 10 mV to perturb the system under quiescent conditions. NOVA 2.1.7 software fits the Nyquist plots obtained to an appropriate equivalent circuit. Before all electrochemical experiments, the additive-manufactured electrodes were activated electrochemically in a 0.5 M NaOH solution, as outlined in the literature.[25] Specifically, the additive-manufactured electrodes were connected as the working electrode (WE), along with a nichrome wire coil counter electrode (CE) and a Ag|AgCl/KCl (3 M) reference electrode (RE), immersed in a 0.5 M NaOH solution. Chronoamperometry was used for activation by applying a voltage of +1.4 V for 200 s, followed by a voltage of −1.0 V for another 200 s. The activated electrodes were then thoroughly rinsed with deionized water and dried using compressed air before further use.

3. RESULTS AND DISCUSSION

The use of new sustainable filaments for electrochemical devices has been growing in recent years.[9] While additive manufacturing, particularly FFF, generates minimal waste, the ongoing dependence on plastic presents environmental challenges and hampers advancements in commercialization. Research has highlighted the potential of cellulose as a valuable additive manufacturing filament for several reasons, primarily due to its favorable crystallinity and ability to enhance filaments' physical properties. Notably, a study by Amorim et al. demonstrated improvements in the electrochemical properties of additive manufacturing filaments by incorporating cellulose acetate as a modifier in an acrylonitrile-butadiene/graphite composite.[22] Their findings indicate an increase in the electroactive area and a faster heterogeneous electron transfer rate constant (k^0_{obs}) when cellulose acetate is included in the filament. This research opens new avenues for understanding the role of cellulose in additive manufacturing filaments and its significance in the development of electrochemical sensors.

3.1. Preparation and Characterization of Microcrystalline Cellulose and Carbon Black Mixed Filament

In this study, we focus on prepare filaments using MCC in a composition of CB/Plasticizer (CO or PEG)/rPLA. MCC is utilized as a replacement for a portion of the plastic (rPLA) in the filament formulation. We compare the electrochemical and physicochemical properties of MCC filaments with those of similar filaments that do not contain cellulose but feature the maximum content of rPLA. A key aspect of our research is the variation of plasticizers, specifically CO and PEG, in the filament composition. It is well-established that CO is a biobased plasticizer, while PEG is a synthetic compound. The combination of CO with MCC is vital for advancing biodegradable filament development. The filaments were produced as shown in Figure 1A. The compounds are mixed at 190 °C for 5 min, then cooled, shredded, and passed through a single-screw extruder to produce the filament. This work produced four distinct filaments. The first two maintain a composition of 20 wt % carbon black (CB), 10 wt % microcrystalline cellulose (MCC), and 60 wt % recycled polylactic acid (rPLA), varying only the plasticizer used, with either 10 wt % castor oil (CO) or 10 wt % PEG referred in the text as MCC/CO and MCC/PEG, respectively. The other two filaments retain the same base composition of 10 wt % CB and 70 wt % rPLA but incorporate either 10 wt % CO or 10 wt % PEG without including MCC, referred to in the text simply as CO and PEG, respectively.

Notably, there was no significant decrease in the flexibility of rPLA, even with the inclusion of MCC, due to the high crystallinity that MCC provides to the filament, as shown in Figure 1B, where we show the exceptional flexibility of MCC/CO filament. Furthermore, all produced filaments displayed exceptional flexibility at low temperatures, as illustrated in Figure S1A for PEG, S1B for CO, and S1C for MCC/PEG. Note that a certain level of filament flexibility is beneficial for achieving optimal printing results with these materials.[23]

Thermogravimetric analyses of the custom filaments are presented in Figure 1C. To compare the results, we evaluated all filaments containing microcrystalline cellulose (MCC) and those that do not, including both virgin rPLA and virgin MCC. Analyzing the thermal properties of both virgin MCC and virgin rPLA is essential for understanding the thermal behavior of the filaments. Furthermore, this analysis can offer insights into the impact of MCC on the stability of the polymer, allowing for accurate determination of the mass of the conductivity filler (CB) present in each filament. The average onset temperature for each filament and the filler contents (wt %) are summarized in Table 1. All filaments exhibit a filler level

Table 1. Evaluation of the Onset of Degradation Temperature, and Filler Percentage for Each of the Bespoke Cellulose/No Cellulose Filaments Produced

filament	average onset of degradation (°C)	filler content (wt %)
MCC/PEG	283 ± 8	21 ± 1
MCC/CO	279 ± 3	23 ± 1
PEG	277 ± 6	20 ± 1
CO	285 ± 4	20 ± 1
virgin MCC	264 ± 6	7 ± 2
virgin rPLA	292 ± 1	1 ± 0.1

ranging from 20 to 23 wt %. We anticipated higher filler level values for those filaments incorporating microcrystalline cellulose (MCC/CO and MCC/PEG), mainly based on the TGA results for virgin cellulose (which indicated a filler level of 7 ± 2 wt %). However, this expectation was not met. The filler content values observed in the composites containing MCC can be attributed to both physical and chemical interactions with the other components used in the filament's manufacture, such as carbon black (CB), recycled polylactic acid (rPLA), and the chosen plasticizer. It is important to note that rPLA constitutes the most significant portion of the filament, accounting for 60 wt %. These values were calculated based on the stabilization of the thermogravimetric analysis (TGA) curve after the degradation of all rPLA, MCC, and plasticizers. The mass of CB added during the thermomixing process was consistently 20 wt % for each filament, indicating minimal loss of material during filament preparation. The degradation temperature of virgin rPLA was found to be 292 ± 1 °C, which is consistent with the literature.

Furthermore, virgin MCC demonstrates a significant weight loss around 320 °C, indicative of substantial changes occurring at that temperature.[24] A slight weight loss of roughly 5 wt % is observed at 100 °C. This initial loss is likely due to the evaporation of water present in MCC.[25,26] The bespoke compositions containing MCC (20%CB/10%MCC/10%CO/60%rPLA (MCC/CO)); 20%CB/10%MCC/10%PEG/60%

https://doi.org/10.1021/acsaenm.5c00233
ACS Appl. Eng. Mater. 2025, 3, 1759−1769

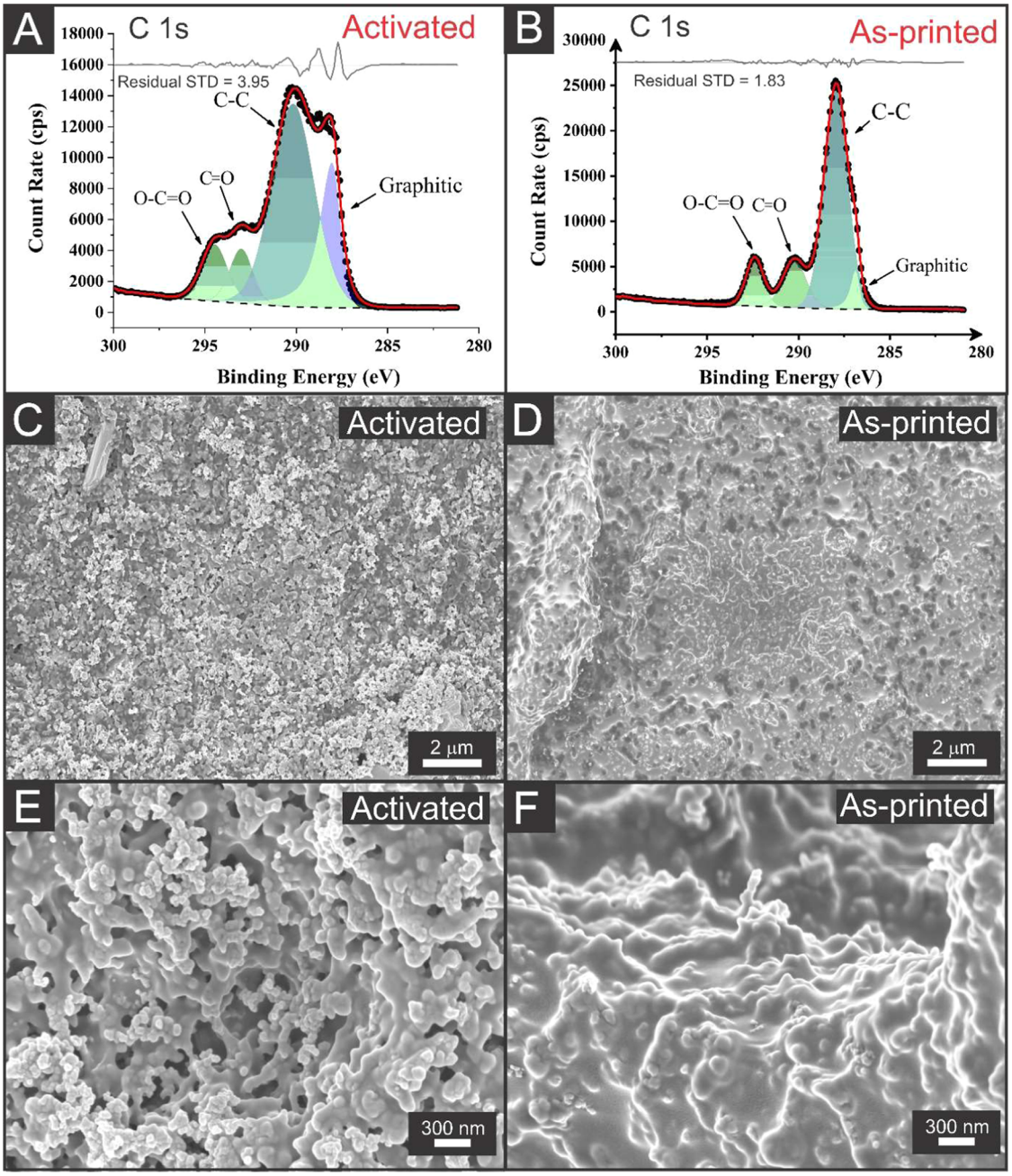

Figure 2. (A) XPS spectra for activated MCC/CO electrode showing the C 1s region and (B) as-printed MCC/CO electrode showing C 1s. (C, D) SEM images for the electrodes at 5k magnification. (E, F) 25k magnification.

rPLA (MCC/PEG)) and those without MCC (20%CB/10% CO/70%rPLA (CO)); 20%CB/10%PEG/70%rPLA (PEG)), each incorporating different plasticizers, exhibited an average onset degradation temperature of approximately 280 °C. As indicated in Table 1, we conclude that while the thermal stability of the filament had a slight decline—an expected outcome, given that the onset temperature of virgin MCC is approximately 264 °C—it does not significantly impact the thermal stability of the composites. The onset temperatures remain close for all composites (approximately 280 °C), suggesting that even with removing 10 wt % of rPLA and adding MCC, the composites still possess adequate thermal stability. This thermal stability effect can be attributed to the barrier properties that CB and MCC provide against gas diffusion from the rPLA.

Other physicochemical characterisations were performed with the electrodes printed from the different filaments. At this stage, it was decided to use only castor oil (CO) as a plasticizer to facilitate the study as the filament performance and printability matched the PEG variation, while also offering the improved sustainability. Since the use of these filaments in electrochemical sensors has been shown to improve after an electrochemical activation step in NaOH medium, the physicochemical characterizations were performed on both as-printed and activated additive-manufactured electrodes. Figure 2A presents the C 1s spectra for the activated electrode obtained using X-ray photoelectron spectroscopy (XPS), while Figure 2B shows the spectra for the as-printed electrode. To achieve an accurate fit, four peaks were identified. The first peak, which is asymmetric, is located at 284.5 eV and is

https://doi.org/10.1021/acsaenm.5c00233
ACS Appl. Eng. Mater. 2025, 3, 1759−1769

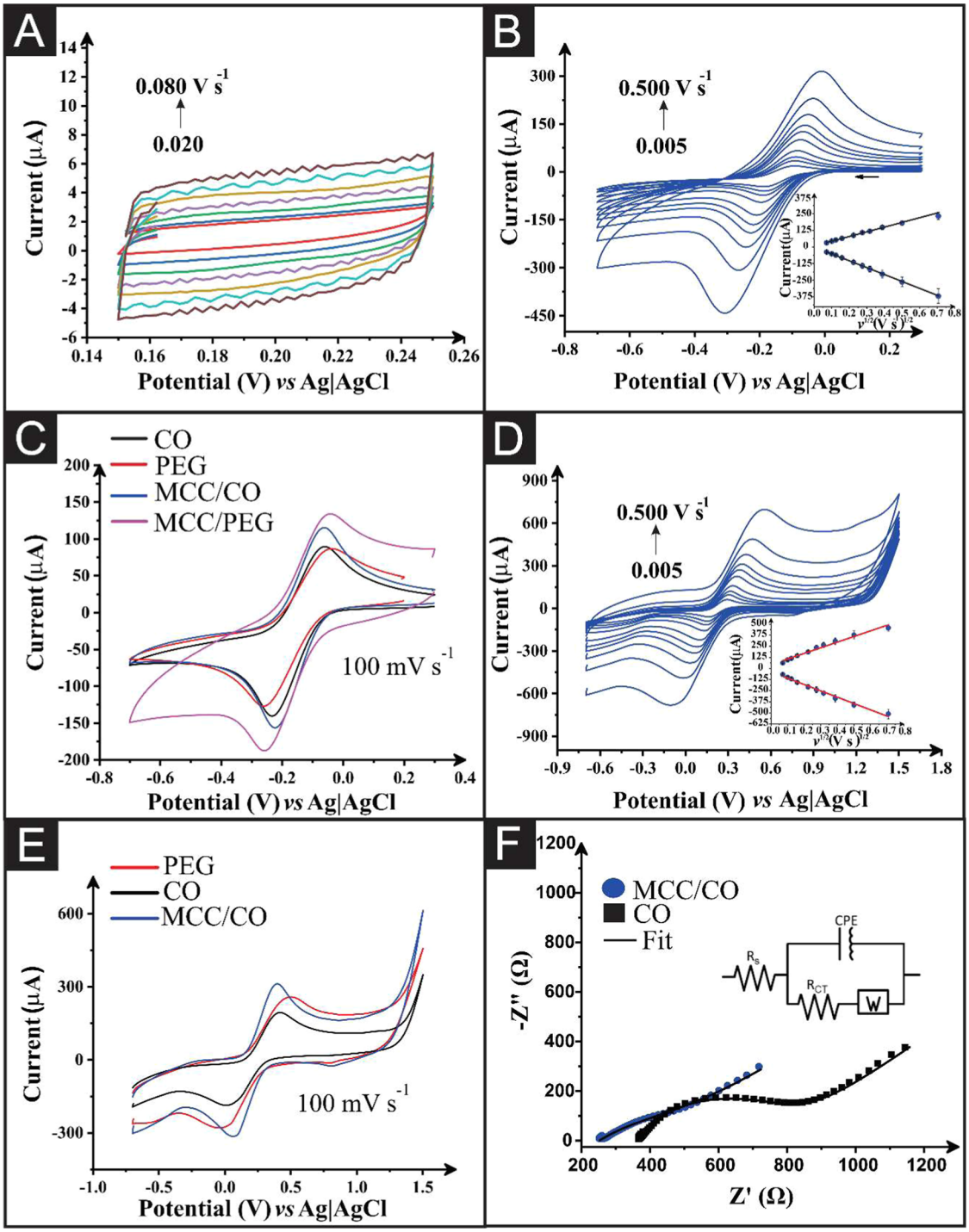

Figure 3. (A) Scan rate study (20−80 mV s^{-1}) of 0.1 M KCl with MCC/CO filament as WE, nickel/chrome as CE and Ag/AgCl/KCl (sat) as RE. (B) Scan rate study (5−500 mV s^{-1}) of $[Ru(NH_3)_6]^{3+}$ (1 mM in 0.1 M KCl) with MCC/CO filament as WE, nickel/chrome as CE and Ag/AgCl (KClsat) as RE. (C) $[Ru(NH_3)_6]^{3+}$ comparison (100 mV s^{-1}) of CO, PEG, MCC/CO and MCC/PEG. (D) Scan rate study (5−500 mV s^{-1}) of $[Fe(CN)_6]^{4-/3-}$ (1 mM in 0.1 M KCl) with MCC/CO filament as WE, nickel/chrome as CE and Ag/AgCl//KCl (sat) as RE. (E) Ferricyanide/Ferrocyanide comparison (100 mV s^{-1}) of CO, PEG, MCC/CO and MCC/PEG. (F) EIS Nyquist plots recorded in 1 mM $[Fe(CN)_6]^{4-/3-}$ and 0.1M KCl.

attributed to the X-ray photoemission of graphitic carbon. Notably, the graphitic peak (284.5 eV) is nearly absent in the XPS data for the as-printed filament. Instead, mainly sp^3 C−C, C═O, and O═C−O bonds are detected, indicating that before activation, the electrode's surface predominantly comprises PLA, CO, and MCC with CB particles located below the depths probed by XPS. The presence of not only PLA on the surface is confirmed by the large C−C bonding peak, as if only PLA was present the three symmetric peaks would be expected to be of similar intensities. This scenario changes upon activation with NaOH, where a large increase in the asymmetric peak at 284.5 eV is observed, aligning with the X-ray photoelectron emission from graphitic carbon. This

https://doi.org/10.1021/acsaenm.5c00233
ACS Appl. Eng. Mater. 2025, 3, 1759−1769

finding suggests the removal of material from the filament's surface, allowing for the introduction of CB.

SEM images of the activated MCC/CO composite (Figure 2C,2E) and the as-printed (Figure 2D,F) were analyzed. In the SEM image of the activated electrode shown in Figure 2C, small spherical particles can be observed on the electrode's surface, which are associated with the carbon black (CB). The surface structure of the activated electrode is more clearly depicted in the SEM image of Figure 2E at a different magnification. Here, the small spheres are connected by fine paths. In contrast, Figure 2F illustrates the mass present between these small spheres, which consists of the rPLA (recycled polylactic acid) that surrounds the CB and MCC.

In Figure S2(A–D), SEM images of the filament composed of CO (without cellulose) at various magnifications are presented. Notably, Figure S1C, which represents the activated electrode, can be compared to Figure 2E to demonstrate significantly more surface material removal. Chemical stabilization of filaments, both with and without MCC, was conducted. Figure S3 illustrates the weight increase of the filaments over 5 days in a 0.1 M KCl solution. It is noteworthy that the mass gain of the filament containing cellulose is greater. This increase in mass is attributed to the chemical properties of cellulose, particularly its structure, which includes polar groups that enhance its interaction with water and the filament itself. Consequently, it is essential to store the filament correctly prior to carrying work out to ensure minimal uptake of atmospheric water.

3.2. Electrochemical Characterization of MCC Filaments and without MCC Filaments

All bespoke filaments with and without MCC were subjected to electrochemical characterization and compared with a commercial CB/PLA filament. The testing utilized additive manufactured electrodes designed in a simple lollipop shape (see Figure S4). This design ensures a consistent connection length, allowing for uniform electrochemical measurements across each test. Figure 3A shows the study of different scan rates of supporting electrolyte (0.1 M KCl) to determine the material's capacitance of MCC/CO. Capacitance is the material's potential to store electric charge in the interface of the material and the solution. The capacitance values were obtained for the two filaments with MCC and without MCC: MCC/CO (75.2 ± 3.0 nF) and CO (84.0 ± 3.2 nF). This value is calculated using the sensitivity of the curves obtained from the relationship between current (μA) vs scan rate (from 20 to 80 mVs^{-1}) and is shown in Figure S5. An example of the cyclic voltammograms obtained with the MCC/CO electrode in the presence of $[Ru(NH3)_6]^{3+}$ (1 mM in 0.1 M KCl) is illustrated in Figure 3B. This particular probe was selected because $[Ru(NH_3)_6]^{3+}$ serves as a near-ideal outer sphere redox probe, facilitating the accurate determination of the heterogeneous electron transfer rate constant (k^0_{obs}) and the effective electrochemical surface area (A_e).

In Table 2, we summarize the electrochemical characterization parameters, including cathodic peak current (I^c_p) and peak-to-peak separation (ΔE_p), measured for $[Ru(NH_3)_6]^{3+}$ at a concentration of 1 mM in 0.1 M KCl, utilizing a scan rate of 100 mV s^{-1}. We also present the calculated k^0_{obs} and A_e. A detailed summary of the key data obtained from this study is provided in Table 2, and the comparison between cyclic voltammograms obtained at the same scan rate is illustrated in Figure 3C. Notably, as shown in Table 2, all filaments

Table 2. Comparison of the Cathodic Peak Currents ($-I^c_p$), Peak-to-Peak Separations (ΔE_p), Heterogeneous Electron Transfer Constant (k^0_{obs}), and Electrochemically Active Area (A_e) All Calculated from Cyclic Voltammograms Recorded in $[Ru(NH_3)_6]^{3+}$ for MCC/PEG, MCC/CO, PEG, CO, and Commercial CB/PLA Filaments

Filament	$-I^c_p$ (μA)[a]	ΔE_p (mV)[a]	$k^0_{obs} \times 10^{-3}$ (cm s^{-1})[b]	A_e (cm^2)[b]
MCC/PEG	166 ± 14	210 ± 4	1.01 ± 0.04	0.69 ± 0.07
MCC/CO	166 ± 23	160 ± 14	1.55 ± 0.05	0.65 ± 0.09
PEG	122 ± 5	221 ± 11	0.90 ± 0.08	0.50 ± 0.01
CO	154 ± 12	180 ± 12	1.31 ± 0.13	0.59 ± 0.035
commercial CB/PLA	73 ± 4	394 ± 13	0.19 ± 0.02	0.36 ± 0.02

[a]Extracted from 100 mV s^{-1} cyclic voltammogram of $[Ru(NH_3)_6]^{3+}$ (1 mM in 0.1 M KCl); [b]Calculated from the $[Ru(NH_3)_6]^{3+}$ scan rate study (5–500 mV s^{-1}).

produced with MCC demonstrated superior electrochemical performance. This enhanced performance of the filament can be attributed to the reduction in the mass of rPLA in the formulation, along with the incorporation of MCC in the filament. It is important to note that all of the bespoke filaments significantly outperformed the commercially available filament. Other works within the literature show an improvement over commercial filament, however they all utilize a larger amount of conductive material. The commercial filament is quoted to contain ∼21 wt % CB, whereas the bespoke filaments produced herein use only 20 wt %. Therefore, we can conclude that the inclusion of MCC is not only improving the sustainability of the filament but also helping to improve the electrochemical performance. There was also a significant improvement shown by the filaments using the CO as a plasticizer over the PEG, once more highlighting how choosing a more sustainable approach can lead to improvements in performance.

The trends observed with $[Ru(NH_3)_6]^{3+}$ were pronounced; however, the majority of electroanalytical targets do not resemble ideal outer-sphere probes. Consequently, it is crucial to characterize electrode materials for inner-sphere probes. To this end, we assessed electrodes from all five filaments using the widely utilized 1 mM $[Fe(CN)_6]^{4-/3-}$ probe in 0.1 M KCl. We measured key electrochemical parameters, including the anodic peak current (I^a_p) and peak-to-peak separation (ΔE_p), for 1 mM $[Fe(CN)_6]^{4-/3-}$ in 0.1 M KCl using a scan rate of 100 mV s^{-1}. We also provided the calculated values for k^0, A_e, solution resistance (R_S), charge-transfer resistance (R_{CT}), and filament resistance (Ω) shown in Table 3. Figure 3D presents a scan rate study conducted with the MCC/CO electrode, ranging from 5 to 500 mV s^{-1}. The cyclic voltammetry plots at a scan rate of 100 mV s^{-1} are shown in Figure 3E for three different filaments: MCC/CO, CO, and PEG. As indicated in Figure 3E, the filament containing MCC exhibited a similar trend to that of the $[Ru(NH_3)_6]^{3+}$ probe, achieving the best values of I^a_p (263 ± 28), ΔE_p (347 ± 11), and, as summarized in Table 3, the optimal k^0_{obs} 0.35 (±0.03) × 10^{-3} cm s^{-1} and A_e (1.16 ± 0.10 cm^2) compared to the other filaments, including commercial filament (protopasta). It is important to emphasize that the bespoke filaments used in this work do not include an increased amount of CB than the commercial filament. The performance of electrodes with MCC (MCC/CO) was further evaluated against those without MCC (CO) through electrochemical impedance spectroscopy (EIS). By fitting the

https://doi.org/10.1021/acsaenm.5c00233
ACS Appl. Eng. Mater. 2025, 3, 1759–1769

Table 3. Summary of the Electrochemical Results Obtained for the Testing of Filaments, Including the Anodic Peak Current (I_p^a) and Peak-to-Peak Separation (ΔE_p), Heterogeneous Electron (Charge) Transfer Rate Constant (k_{obs}^0),Electrochemically Active Area(A_e), solution resistance (R_S) and charge-transfer resistance (R_{CT}). All Calculated from Cyclic Voltammograms Recorded in $[Fe(CN)_6]^{4-/3-}$ (1 mM in 0.1 M KCl)[a,b,c,d,e,f,g]. The solution resistence (R_s) and charge-transfer resistence(R_{CT}) from EIS in $[Fe(CN)_6]^{4-/3-}$(1 mM in 0.1 M KCl)[e,f].

filament	I_p^a (μA)[a]	ΔE_p (mV)[b]	k_{obs}^0 ($\times 10^3$ cm s^{-1})[c]	A_e (cm^2)[d]	R_S (Ω)[e]	R_{CT} (kΩ)[f]	R (kΩ)[g]
MCC/PEG	261 ± 52	514 ± 52	0.18 ± 0.06	1.15 ± 0.13	-	-	1.60 ± 0.1
MCC/CO	263 ± 28	347 ± 11	0.35 ± 0.03	1.16 ± 0.10	263 ± 11	207 ± 32	1.16 ± 0.1
PEG	216 ± 20	523 ± 13	0.14 ± 0.05	0.98 ± 0.11	-	-	2.36 ± 0.3
CO	198 ± 17	369 ± 12	0.27 ± 0.06	0.92 ± 0.10	332 ± 46	579 ± 15	1.25 ± 0.1
commercial CB/PLA	93 ± 12	837 ± 50	0.01 ± 0.01	0.48 ± 0.06	2843 ± 2000	7378 ± 540	3.90 ± 0.5

[a,b]Extracted from 100 mV s^{-1} cyclic voltammograms of Ferri/Ferro (1 mM in 0.1 M KCl). [c,d]Calculated from the Ferri/Ferro scan rate study (5–500 mV s^{-1}). [e,f]Extracted from Nyquist plots of EIS experiments in a solution of Ferri/Ferro (1 mM in 0.1 M KCl). [g]Resistance measured with a multimeter across 10 cm of filament.

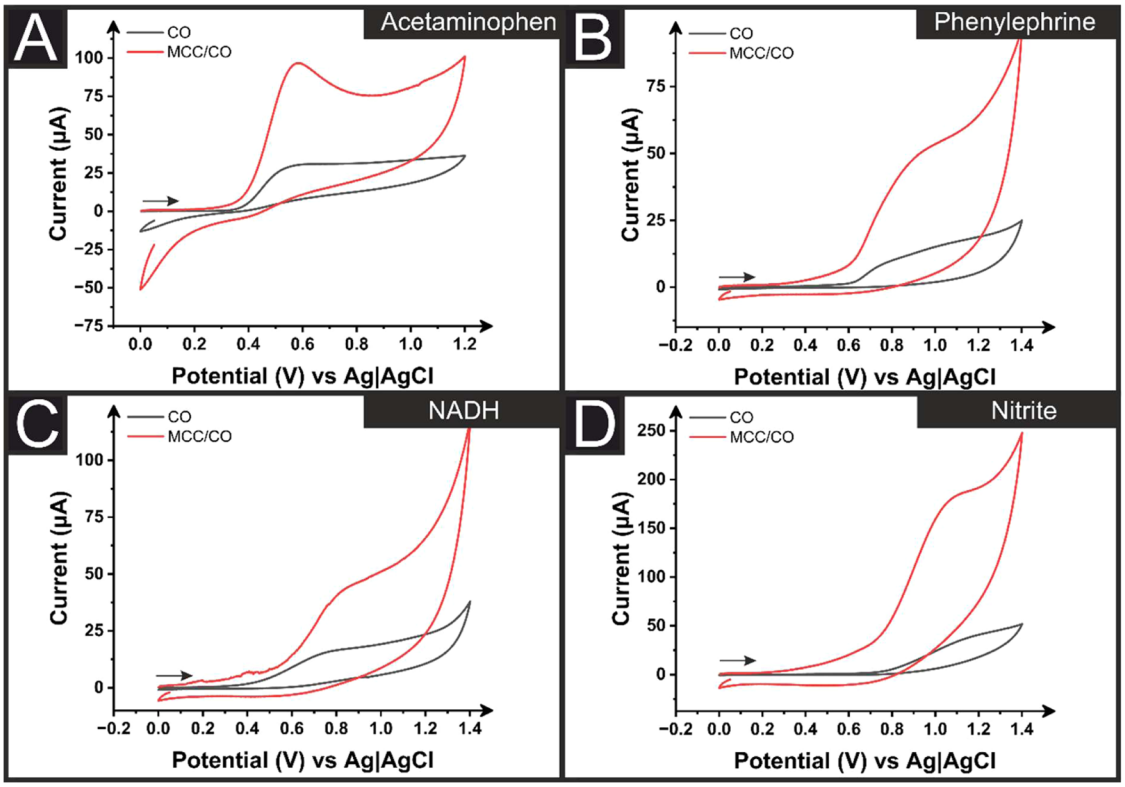

Figure 4. CV (50 mV s^{-1}) scans performed with a MCC/CO and CO additive-manufactured electrodes as the working electrode, nichrome wire counter and Ag|AgCl reference electrode for the detection of 500 μM of (A) acetaminophen, (B) phenylephrine, (C) NADH, and (D) nitrite.

obtained Nyquist plots with the appropriate equivalent circuit, we calculated the solution resistance (R_S) and charge-transfer resistance (R_{CT}). Figure 3F illustrates the obtained Nyquist plots, accompanied by an equivalent circuit, while the calculated R_S and R_{CT} values are summarized in Table 3. The values of R_S and R_{CT} for the electrode containing MCC showed the minimum resistance compared to others. These findings are consistent with the filament resistances and align with the electrochemical characterization results for both filaments, with and without MCC.

3.3. Electroanalytical Performance

After assessing the physicochemical characteristics and electrochemical properties of the MCC/CO additive-manufactured electrodes, their response to different analytes was tested and compared to electrodes printed without MCC. Figure 4 shows the CV response at 50 mV s^{-1} of the MCC/CO and CO electrodes toward acetaminophen (500 μM, Figure 4A), phenylephrine (500 μM, Figure 4B), NADH (500 μM, Figure 4C), and nitrite (500 μM, Figure 4D).

In each case, there is a clear improvement in the peak shape obtained for every analyte in addition to a large increase in the peak current. For acetaminophen, Figure 4A, the peak current increased from 30 ± 2 μA with the CO electrode to 96 ± 4 μA with the MCC/CO electrode. Similar trends were seen for phenylephrine, an increase from 16 ± 2 to 41 ± 4 μA, NADH, an increase from 11 ± 2 to 42 ± 2 μA, and nitrite, an increase from 37 ± 5 to 120 ± 6 μA. This highlights how the inclusion of MCC within the filament has significantly improved the electroanalytical response to a wide range of analytes.

Following this initial study on the performance of the electrodes, we selected MCC/CO for quantifying dopamine (DPA) in human serum providing full proof-of-concept. DPA is a crucial biomolecule that plays a significant role in human

https://doi.org/10.1021/acsaenm.5c00233
ACS Appl. Eng. Mater. 2025, 3, 1759–1769

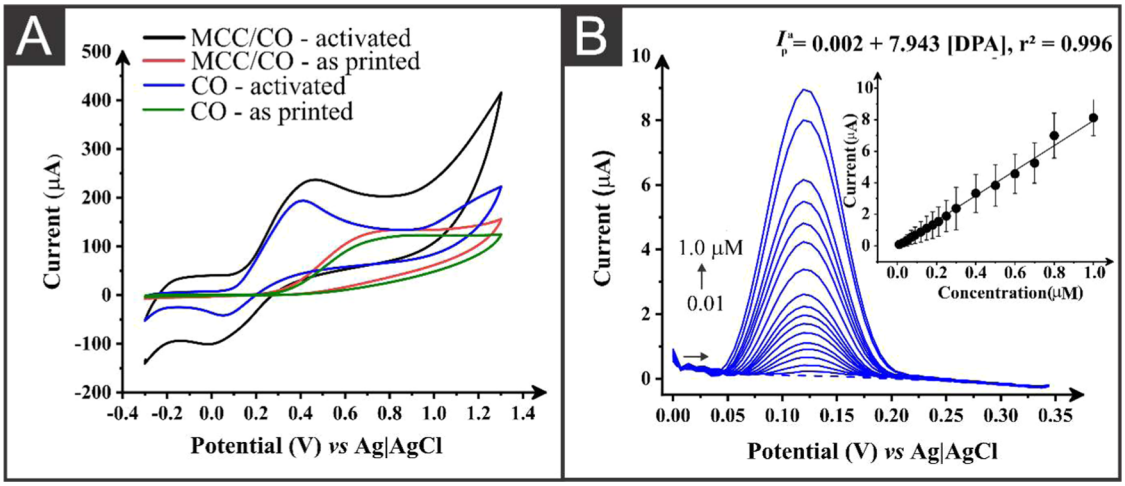

Figure 5. (A) Cyclic voltammograms of 1 mM of dopamine (DPA) in 0.1 M phosphate buffer (pH 7.2) in different electrodes: MCC/CO activated (black), MCC/CO as-printed (red), CO activated (blue), and CO as-printed (green). Scan rate: 100 mV s^{-1}. (B) MCC/CO in PBS pH 7.2 in a concentration range of 0.01 to 1.0 μM. Inset: the calibration plot. DPV parameters: amplitude: 90 mV and step potential: 7 mV.

metabolism and is linked to various neurological disorders, including Parkinson's disease and schizophrenia.[27] Furthermore, to explore the significance of MCC in the filament, we also evaluated the two filaments with and without cellulose, in both activated and as-printed states, for their potential in DPA detection using the cyclic voltammetry technique. Figure 5A shows cyclic voltammograms obtained from two different electrodes, with and without MCC, both activated with NaOH and as-printed. The electrode containing MCC exhibited the best response to dopamine when activated (black voltammogram) with NaOH, with an oxidation peak at 0.35 V and a reduction peak at 0.00 V. Similar peaks were observed in the activated electrode made without cellulose; however, the current peaks (I_p^a and I_p^c) were more intense in the MCC activated electrode. Therefore, the activated MCC/CO filament was used for DPA determination.

The quantification of DPA was then studied using differential pulse voltammetry (DPV). First, DPV parameters were optimized, as shown in Figures S6 and S7, with the best results obtained using a step potential of 7 mV and an amplitude of 90 mV. Then, optimized DPV was used to produce the analytical curves for the detection of DPA using an activated MCC electrode, shown in Figure 5B, and an activated electrode without MCC, in Figure S8.

A summary of the results obtained is presented in Table 4. The oxidation peak current exhibited a linear increase with DPA concentration in both cases, with a linear range of 0.01 to 1.0 μM. The MCC electrode exhibited a linear equation of I (μA) = 7.9C_{DPA} (μM) + 0.002 (R = 0.996), against I (μA) = 2.5C_{DPA} (μM) − 0.012 (R = 0.955) for the electrode without MCC. The MCC/CO filament delivered enhanced electroanalytical outcomes, achieving a sensitivity of 7.943 μA μM^{-1}, three times greater than the filament without MCC, and a limit of detection (LOD) of 3.0 nM and a limit of quantification (LOQ) of 0.01 μM. The increase in the LOD and LOQ values are attributed to the increased capacitance seen in the baseline for this electrode. These findings align well with other electrochemical sensors for DPA detection reported in the literature, as summarized in Table S1.

Table 4. Comparison of Analytical Results for Dopamine Using the Optimized DPV Method, Obtained from CO and MCC/CO

Parameters	CO	MCC/CO
linear range (μM)	0.01−1.0	0.01−1.0
slope (μA μM^{-1})	2.539	7.943
intercept (μA)	0.012	0.002
R^2	0.955	0.996
LOD[a] (nM)	1.2	3.0
LOQ[b] (nM)	4	10

[a]LOD = 3 x (StDev/slope). [b]LOQ = 10 x (StDev/slope).

The DPA quantification was performed using a spiked human serum sample, as illustrated in Figure 6, to mimic the application of the electroanalytical sensing platform in real-world scenario. In this test, a concentration of 10 μM of DPA of stock solution was prepared in phosphate buffer pH 7.2. Then, the human serum was then diluted 500-fold in the supporting electrolyte. The standard addition method was utilized for DPV measurements. A commendable recovery rate of 102.4 ± 6.1% was achieved, highlighting the effectiveness of incorporating cellulose into the filament for the electroanalytical sensing platform used to detect dopamine in human serum.

4. CONCLUSIONS

This work describes the first production of conductive additive manufacturing filaments by adding microcrystalline cellulose (MCC) within a polymeric matrix containing recycled poly(lactic acid) (rPLA), reducing the plastic content by 10 wt %. The addition of MCC did not have any adverse effect on the low-temperature flexibility or printability of the filament. After extensive physicochemical and electrochemical characterization, it was shown that the inclusion of MCC improved the performance of the filament toward both inner and outer-proofosphere redox probes. Significantly, all electrodes with MCC showed an enhanced electrochemical performance when compared to the commercially available conductive filament, even though there was less conductive filler present. Dopamine was chosen as a proof of concept for the electroanalytical application, obtaining sensitivity values of 7.943 μA μM^{-1}, a LOD of 3 nM, and a LOQ of 10 nM. This work shows how

https://doi.org/10.1021/acsaenm.5c00233
ACS Appl. Eng. Mater. 2025, 3, 1759−1769

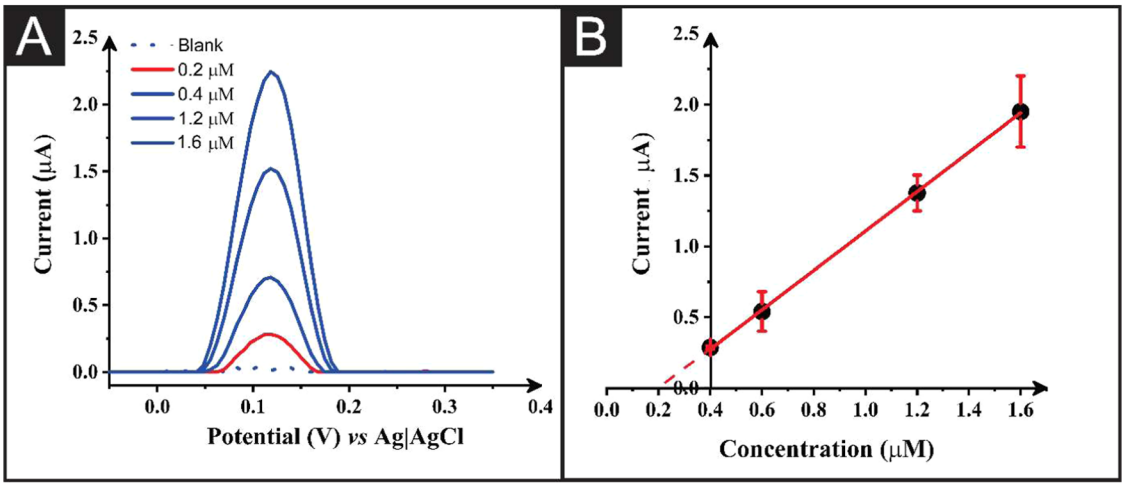

Figure 6. (A) DPV measurements of spiked (A) in human serum (red line) diluted (500-fold) in Phosphate buffer pH 7.2 with subsequent additions of dopamine standard solutions (0.4 to 1.6 μM) (blue lines), and (B) the respective calibration curve. DPV parameters: amplitude: 90 mV and step potential: 7 mV. Measurements were carried out using MCC/CO.

improving the sustainability of processes can, in some cases, also enhance their performance for the desired applications.

■ ASSOCIATED CONTENT

Supporting Information

The Supporting Information is available free of charge at https://pubs.acs.org/doi/10.1021/acsaenm.5c00233.

Photographs of the produced filament, SEM micrographs of the electrode surfaces, ingress study, photographs of printed electrodes, electrochemical and electroanalytical application optimization plots, table of comparison to literature (PDF)

■ AUTHOR INFORMATION

Corresponding Author

Craig E. Banks − *Faculty of Science and Engineering, Manchester Metropolitan University, Manchester M1 5GD, Great Britain;* orcid.org/0000-0002-0756-9764; Phone: +44(0)1612471196; Email: c.banks@mmu.ac.uk

Authors

Bruno Ferreira − *Faculty of Science and Engineering, Manchester Metropolitan University, Manchester M1 5GD, Great Britain; Departamento de Química Fundamental, Instituto de Química, Universidade de São Paulo, São Paulo, SP 05508-000, Brazil*

Elena Bernalte − *Faculty of Science and Engineering, Manchester Metropolitan University, Manchester M1 5GD, Great Britain*

Robert D. Crapnell − *Faculty of Science and Engineering, Manchester Metropolitan University, Manchester M1 5GD, Great Britain;* orcid.org/0000-0002-8701-3933

Karen K. L. Augusto − *Faculty of Science and Engineering, Manchester Metropolitan University, Manchester M1 5GD, Great Britain; Laboratório de Analítica, Bioanalítica, Biossensores, Eletroanalítica e Sensores, Departamento de Química, Universidade Federal de São Carlos(UFSCar), São Carlos, SP 13560-970, Brazil*

Uday Lomesh − *Faculty of Science and Engineering, Manchester Metropolitan University, Manchester M1 5GD, Great Britain; Thapar Institute of Engineering and Technology, Patiala, Punjab 147004, India*

Muhzamil A. Khan − *Faculty of Science and Engineering, Manchester Metropolitan University, Manchester M1 5GD, Great Britain;* orcid.org/0009-0001-3960-9310

Orlando Fatibello-Filho − *Laboratório de Analítica, Bioanalítica, Biossensores, Eletroanalítica e Sensores, Departamento de Química, Universidade Federal de São Carlos(UFSCar), São Carlos, SP 13560-970, Brazil*

Thiago R.L.C. Paixão − *Departamento de Química Fundamental, Instituto de Química, Universidade de São Paulo, São Paulo, SP 05508-000, Brazil;* orcid.org/0000-0003-0375-4513

Complete contact information is available at: https://pubs.acs.org/10.1021/acsaenm.5c00233

Notes

The authors declare no competing financial interest.

■ ACKNOWLEDGMENTS

This research was supported by São Paulo Research Foundation (FAPESP) (Grant numbers: 2023/00246-1 and 2024/04116−8), Coordenação de Aperfeiçoamento de Pessoal de Nível Superior-Brasil (CAPES) (Grant numbers: 88887.601733/2021-00, CAPES-Print 88887.836030/2023−00 and Finance Code 001), Conselho Nacional de Desenvolvimento Científico e Tecnológico (Grant number: 311847-2018-8, 302839/2020-8, 140406/2021−2, 401681/2023−8, 405620/2021-7 (Universal), INCT NanoVida (grant 406079/2022−6) and INCTBio (grant 465389/2014-7)).

■ REFERENCES

(1) Silva, L. R. G.; Bertolim, L. V.; Stefano, J. S.; Bonacin, J. A.; Richter, E. M.; Munoz, R. A. A.; Janegitz, B. C. New route for the production of lab-made composite filaments based on soybean oil, polylactic acid and carbon black nanoparticles, and its application in the additive manufacturing of electrochemical sensors. *Electrochim. Acta* **2025**, *513*, No. 145566.

(2) Siqueira, G. P.; de Faria, L. V.; Swain, K. K.; Trindade, M. A. G.; Richter, E. M.; Muñoz, R. A. A. 3D-printed electrochemical sensors. In *3D Printing in Analytical Chemistry*; Herrero-Martínez, J. M.; Miró,

M.; Carrasco-Correa, E. J.; Vergara-Barberán, M., Eds.; Elsevier, 2025; Chapter 15, pp 355−391.
(3) Carvalho, M. S.; Rocha, R. G.; Nascimento, A. B.; Araújo, D. A. G.; Paixão, T. R. L. C.; Lopes, O. F.; Richter, E. M.; Muñoz, R. A. A. Enhanced electrochemical performance of 3D-printed electrodes via blue-laser irradiation and (electro)chemical treatment. *Electrochim. Acta* **2024**, *506*, No. 144995.
(4) Abdalla, A.; Patel, B. A. 3D Printed Electrochemical Sensors. *Annu. Rev. Anal. Chem.* **2021**, *14*, 47−63.
(5) Kumar, S.; Singh, H.; Singh, I.; Bharti, S.; Kumar, D.; Siebert, G.; Koloor, S. S. R. A comprehensive review of FDM printing in sensor applications: Advancements and future perspectives. *J. Manuf. Processes* **2024**, *113*, 152−170.
(6) Crapnell, R. D.; Kalinke, C.; Silva, L. R. G.; Stefano, J. S.; Williams, R. J.; Munoz, R. A. A.; Bonacin, J. A.; Janegitz, B. C.; Banks, C. E. Additive manufacturing electrochemistry: an overview of producing bespoke conductive additive manufacturing filaments. *Mater. Today* **2023**, *71*, 73−90.
(7) Sigley, E.; Kalinke, C.; Crapnell, R. D.; Whittingham, M. J.; Williams, R. J.; Keefe, E. M.; Janegitz, B. C.; Bonacin, J. A.; Banks, C. E. Circular economy electrochemistry: creating additive manufacturing feedstocks for caffeine detection from post-industrial coffee pod waste. *ACS Sustainable Chem. Eng.* **2023**, *11* (7), 2978−2988.
(8) Long, L.; Wang, S.; Xiao, M.; Meng, Y. Polymer electrolytes for lithium polymer batteries. *J. Mater. Chem. A* **2016**, *4* (26), 10038−10069.
(9) Katcharava, Z.; Marinow, A.; Bhandary, R.; Binder, W. H. 3D Printable Composite Polymer Electrolytes: Influence of SiO2 Nanoparticles on 3D-Printability. *Nanomaterials* **2022**, *12* (11), No. 1859.
(10) Kodal, M.; Sirin, H.; Ozkoc, G. Long- and short-term stability of plasticized poly(lactic acid): effects of plasticizers type on thermal, mechanical and morphological properties. *Polym. Bull.* **2019**, *76* (1), 423−445.
(11) Crapnell, R. D.; Arantes, I. V. S.; Whittingham, M. J.; Sigley, E.; Kalinke, C.; Janegitz, B. C.; Bonacin, J. A.; Paixão, T. R. L. C.; Banks, C. E. Utilising bio-based plasticiser castor oil and recycled PLA for the production of conductive additive manufacturing feedstock and detection of bisphenol A. *Green Chem.* **2023**, *25* (14), 5591−5600.
(12) Wuamprakhon, P.; Crapnell, R. D.; Sigley, E.; Hurst, N. J.; Williams, R. J.; Sawangphruk, M.; Keefe, E. M.; Banks, C. E. Recycled Additive Manufacturing Feedstocks for Fabricating High Voltage, Low-Cost Aqueous Supercapacitors. *Adv. Sustainable Syst.* **2023**, *7* (2), No. 2200407.
(13) Gauss, C.; Pickering, K. L.; Muthe, L. P. Composites Part C: Open Access.
(14) Yao, X.; Zhang, S.; Wei, N.; Qian, L.; Coseri, S. Cellulose-based conductive hydrogels for emerging intelligent sensors. *Adv. Fiber Mater.* **2024**, *6* (5), 1256−1305.
(15) Sheraz, M.; Sun, X.-F.; Siddiqui, A.; Wang, Y.; Hu, S.; Sun, R. Cellulose-Based Electrochemical. *Sensors* **2025**, *25* (3), No. 645.
(16) Zhou, L.; Ke, K.; Yang, M.-B.; Yang, W. Recent progress on chemical modification of cellulose for high mechanical-performance Poly(lactic acid)/Cellulose composite: A review. *Compos. Commun.* **2021**, *23*, No. 100548.
(17) Moon, R. J.; Martini, A.; Nairn, J.; Simonsen, J.; Youngblood, J. Cellulose nanomaterials review: structure, properties and nanocomposites. *Chem. Soc. Rev.* **2011**, *40* (7), 3941−3994.
(18) Bangar, S. P.; Esua, O. J.; Nickhil, C.; Whiteside, W. S. Microcrystalline cellulose for active food packaging applications: A review. *Food Packag. Shelf Life* **2023**, *36*, No. 101048.
(19) Mathew, A. P.; Oksman, K.; Sain, M. Mechanical properties of biodegradable composites from poly lactic acid (PLA) and microcrystalline cellulose (MCC). *J. Appl. Polym. Sci.* **2005**, *97* (5), 2014−2025.
(20) Tomec, D. K.; Schöflinger, M.; Leßlhumer, J.; Centa, U. G.; Žigon, J.; Kariž, M. The Effects of Microcrystalline Cellulose Addition on the Properties of Wood−PLA Filaments for 3D Printing. *Polymers* **2024**, *16* (6), No. 836.
(21) Incarnato, L.; Nobile, M. R.; Scarfato, P. Development of PLA/microcellulose Biocomposite Filaments for 3D Printing. *Macromol. Symp.* **2022**, *405*, No. 2100250, DOI: 10.1002/masy.202100250.
(22) Amorim, P. H. O.; Oliveira, F. Q.; dos Santos, H. C.; Pereira, R. P.; Dornellas, R. M.; Semaan, F. S. Cellulose Acetate/ABS Blends as Insulating Phases for 3D Printing of Carbon-based Composite Sensors. In *Smart Innovation, Systems and Technologies*; Springer, 2021; pp 249−258.
(23) dos Santos, F. A.; Iulianelli, G. C. V.; Tavares, M. I. B. Effect of microcrystalline and nanocrystals cellulose fillers in materials based on PLA matrix. *Polym. Test.* **2017**, *61*, 280−288.
(24) Uesu, N. Y.; Pineda, E. A. G.; Hechenleitner, A. A. W. Microcrystalline cellulose from soybean husk: effects of solvent treatments on its properties as acetylsalicylic acid carrier. *Int. J. Pharm.* **2000**, *206* (1), 85−96.
(25) Fielden, K. E.; Newton, J. M.; O'Brien, P.; Rowe, R. C. Thermal Studies on the Interaction of Water and Microcrystalline Cellulose. *J. Pharm. Pharmacol.* **1988**, *40* (10), 674−678.
(26) Loof, D.; Hiller, M.; Oschkinat, H.; Koschek, K. Quantitative and Qualitative Analysis of Surface Modified Cellulose Utilizing TGA-MS. *Materials* **2016**, *9* (6), No. 415.
(27) Kim, Y.-R.; Bong, S.; Kang, Y.-J.; Yang, Y.; Mahajan, R. K.; Kim, J. S.; Kim, H. Electrochemical detection of dopamine in the presence of ascorbic acid using graphene modified electrodes. *Biosens. Bioelectron.* **2010**, *25* (10), 2366−2369.

https://doi.org/10.1021/acsaenm.5c00233
ACS Appl. Eng. Mater. 2025, 3, 1759−1769